HOKKAIDO UNIVERSITY

Title	Silver-modulated SiO2-supported copper catalysts for selective hydrogenation of dimethyl oxalate to ethylene glycol
Author(s)	Huang, Ying; Ariga, Hiroko; Zheng, Xinlei; Duan, Xinping; Takakusagi, Satoru; Asakura, Kiyotaka; Yuan, Youzhu
Citation	Journal of catalysis, 307, 74-83 https://doi.org/10.1016/j.jcat.2013.07.006
Issue Date	2013-11
Doc URL	http://hdl.handle.net/2115/54629
Type	article (author version)
File Information	JC_MS 20130424.pdf

Instructions for use

Hokkaido University Collection of Scholarly and Academic Papers : HUSCAP

Silver-modulated SiO_2-supported copper catalysts for selective hydrogenation of dimethyl oxalate to ethylene glycol

Ying Huang,[1] Hiroko Ariga,[2] Xinlei Zheng,[1] Xinping Duan,[1] Satoru Takakusagi,[2] Kiyotaka Asakura[2]*, Youzhu Yuan[1]*

[1] *State Key Laboratory of Physical Chemistry of Solid Surfaces and National Engineering Laboratory for Green Chemical Production of Alcohols-Ethers-Esters, College of Chemistry and Chemical Engineering, Xiamen University, Xiamen 361005, China*

[2] *Catalysis Research Center, Hokkaido University, Kita-ku N21W10, Sapporo, Hokkaido 001-0021, Japan*

* To whom correspondence should be addressed. E-mail: yzyuan@xmu.edu.cn, Tel: +86-592-2181659, Fax: +86 592 2183047, or E-mail: askr@cat.hokudai.ac.jp, Tel & Fax: +81-11-706-9113.

Abstract

A SiO_2-supported bimetallic catalyst composed of copper (Cu) and a small amount of silver (Ag) by a one-step urea-assisted gelation method shows remarkable enhancements in catalytic performance for selective hydrogenation of dimethyl oxalate (DMO) to ethylene glycol (EG). Coupling with a series of ~~characteristics~~ characterization and kinetic studies, the improved activity is rationalized essentially due to the formation of Ag nanoclusters and Cu-Ag alloys involved in Cu nanoparticles on SiO_2 surface. The coherent interactions between Cu and Ag species are beneficial for creating the active Cu^+/Cu^0 species in a suitable proportion and restraining the transmigration of bimetallic nanoparticles during the hydrogenation process. In particular, an optimized Cu-Ag/SiO_2 catalyst with Ag/Cu atomic ratio of 0.05 that generates a balanced Cu^+/Cu^0 proportion and highly dispersed bimetal particles affords the highest turnover frequency, over 97.0% EG selectivity and excellent catalytic stability longer than 150 h for the DMO hydrogenation to EG.

Keywords: Copper; Silver; Hydrogenation; Dimethyl oxalate; Ethylene glycol.

1. Introduction

Ethylene glycol (EG) is an important chemical that widely used as antifreezer, polyester fibers, solvents and so on [1]. However, the exhausting of crude oil resources and the increasing demand for EG urge a new promising approach for the synthesis of EG to substitute the traditional petroleum-derived one [2,3]. One of the possible approaches, the so-called coal to EG (CTE), is relatively green and economical. The CTE process involves gasification of coal to syngas, followed by the coupling of CO with nitrite esters to oxalates, and then the hydrogenation of oxalates to EG [1,4,5]. Selective hydrogenation of dimethyl oxalate (DMO) to EG as one of the key reactions for CTE route had drew tremendous attentions. Although great effort has been made to study the DMO hydrogenation process, many problems still leave to be solved. At present, the EG selectivity and catalytic stability remain to be improved, the perception of active sites is still controversial and the essence of catalyst deactivation needs further elucidation. More understanding and generic concepts for a more rationalcatalyst design is highly desirable.

Cu-based catalysts have been studied extensively for vapor-phase hydrogenation of DMOsince they allow for selective hydrogenation of carbon-oxygen bonds and are relatively inactive in carbon-carbon bond hydrogenolysis [6]. So far, Cu-Cr catalysts have been still the preferred industrial catalysts for the CTE process because of their relatively high catalytic activity and long lifetime [7–9]. However, the use of toxic chromium will endanger the safety of environment and the security of workers. Therefore, different carriers (e.g., SiO_2, Al_2O_3 and ZnO) for Cr-free Cu-based catalysts were evaluated [10–12], among which the

Cu/SiO_2 catalystshowed the highest EG yield and was considered a potential alternative for the conventional CuCr catalyst. But the Cu/SiO_2 catalyst is relatively sintering-nonresistant and mechanically unstable for industrial operation [6,13–16]. Thus, considerable efforts are focused on modifying Cu/SiO_2 catalyst by various methods, including adding a second species [13–16], adopting different preparation methods [3,17–21], and using different structures of silica support [22–26]. Cu, Ag and Au are coinage metals in the same group of the periodic table, they all possess the face-centered cubic (fcc) structure with close lattice parameters, and their electronic structure and physical chemical properties are similar. They can form intermetallic or alloy phase with each other. Synergistic effect between Cu-Au [27,28], Cu-Ag [29,30], Au-Ag [31,32] bimetallic catalysts have been reported. Interestingly, recent results show that a bimetallic Cu-Au catalyst with large amount of Au could present improved performance in the DMO hydrogenation to MG [33], while that with small amount of Au exhibited remarkable enhancements in activity and stability for the DMO hydrogenation to EG [34]. Spectroscopic studies revealed that Cu-Au alloy nanoparticles (NPs) were formed on the catalyst surfaces, which were believed to be beneficial for retarding the surface transmigration of Cu species during the hydrogenation process. Further, the surface Cu^+ and Cu^0 proportion would be varied according to the amount of incorporated Au, showing different catalytic behaviors under same conditions as a result. The catalytic performance of Cu-Ag/SiO_2 catalysts prepared by a deposition-precipitation method has also been evaluated for the DMO hydrogenation reaction, affording MG as the main product [35]. However, the structure and the structure-activity relationship of the Cu-Ag catalysts are

ambiguous.

In this work, we incorporate a small amount of Ag into Cu/SiO_2 through a urea-assisted gelation method and find that the bimetallic $Cu\text{-}Ag/SiO_2$ catalysts are efficient for hydrogenation of DMO to EG. Kinetic and spectroscopic studies will show that an intimate interaction between Cu and Ag NPs and a cooperative effect between them might be essentially responsible for the enhanced catalysis.

2. Experimental

2.1. Catalyst preparation

Bimetallic $Cu\text{-}Ag/SiO_2$ catalysts with a presetmetal loading of 10 wt% were prepared by urea-assisted gelation method [13]. Briefly, 4.5 g of 40 wt% LudoxAS-40 colloidal silica was dispersed in 100 mL of aqueous solution containing 6.0 g of urea, a certain amount of $AgNO_3$, $Cu(NO_3)_2{\cdot}3H_2O$ and aqueous ammonia (28 wt%) in a round-bottomed flask. The suspension was vigorously stirred at 353 K in an oil bath for 4 h. The precipitate obtained was separated by hot filtration, washed thrice with deionized water, and dried at 393 K overnight, followed by calcination at 623 K for 4 h. The catalyst precursor was denoted as $Cu_1\text{-}Ag_x/SiO_2$, where x represents atomic ratio of Ag and Cu.

The Cu/SiO_2 catalyst with 10 wt% Cu loading, and the Ag/SiO_2 catalyst with 10 wt% Ag were also prepared by urea-assisted gelation method.

2.2. Catalyst characterizations

N_2 adsorption–desorption isotherms for the catalysts were measured at 77 K using a Micromeritics TriStar II 3020 porosimetry analyzer. The samples were degassed at 573 K for 3 h prior to the measurements. The specific surface area (S_{BET}) was calculated using the Brunauer-Emmett-Teller (BET) method, adopting the isotherm data in a relative pressure (P/P_0) range of 0.05–0.2. The mesopore size distributions were evaluated from the desorption branch of isotherm using the Barrett-Joyner-Halenda (BJH) method. The total pore volume depended on the absorbed N_2 volume at a relative pressure of approximate 0.99. X-ray diffraction (XRD) patterns for the catalyst samples were conducted on a PANalytical X'pert Pro Super X-ray diffractometer using Cu K_α radiation (λ = 0.15418 nm) with a scanning angle (2θ) range of 10–90°, a tube voltage of 40 kV, and a current of 30 mA. For *in situ* XRD measurement, a 5%H_2-95%N_2 mixture was introduced at a flow rate of 50 cm^3 min^{-1}. Temperature ramping programs were performed from room temperature to 523, 573, 623, 673, 723, 773, 873, and 973 Kat a rate of 2 K min^{-1}. The XRD patterns were collected after samples reached the preset temperatures for 30 min. The diffraction pattern was identified by matching them with reference patterns included in the JCPDS data base. The full-width-at-half-maximum of Cu(111) diffraction at a 2θ of 43.2° was used to calculate the Cu crystallite size using the Scherrer equation.

Hydrogen-temperature-programmed reduction (H_2-TPR) for the as-calcined catalyst samples was carried out on a Micromeritics Autochem II 2920 instrument connected to a Hiden Qic-20 mass spectrometer (MS). 100 mg of the calcined catalyst was loaded into a quartz U-tube and dried in an argon stream at 393 K for 1 h. After cooling to room

temperature under argon, a flow of 5%H_2-95% N_2 (50 mL min^{-1}) was fed into the catalyst bed, and then the temperature was ramped linearly from ambient temperature to 1073 K at a rate of 10 K min^{-1}. A 5A zeolite trap was connected to the reactor outlet to remove moisture. Hydrogen consumption was simultaneously monitored by a thermal conductivity detector (TCD) and MS.

Transmission electron microscopy (TEM) images were obtained on a Tecnai F30 apparatus operated at 300 kV. The composition analysis of each metal particle was carried out using energy dispersive X-ray spectroscopy (EDS) at scanning TEM-STEM mode. Catalyst powder was dispersed in ethanol with the assistance of ultrasound at room temperature. The as-obtained solution was dropped onto the carbon coated molybdenum grids.

Ultraviolet-visible diffuse reflectance spectroscopy (UV-vis DRS) of as-reduced catalysts was collected on a UV-vis-NIR Spectrophotometer CARY 5000 scan spectrophotometer. All catalyst precursors were freshly reduced in a 5%H_2-95%N_2 atmosphere at 623 K for 4 h. Then the as-reduced samples were carefully collected under argon atmosphere at room temperature and sealed in glass bottles before UV-vis DRS measurements.

Cu K-edge and Ag K-edge XAFS measurements were performed in a transmission mode at BL12C and NW10 beam line in PF-AR and Photon Factory, Institute of Materials Structure Science, High Energy Accelerator Research Organization (IMSS-KEK), Japan. The storage ring was operated at 2.5 GeV with 450mA in a top-up mode. A Si (111) double

crystal monochromator was used in a quick scan mode. Samples after reduction under 5% H_2-95% Ar at 623 K for 2 h were sealed in the glass cells under He(Cu) or Ar(Ag) and XAFS spectra were taken at room temperature. The analysis of EXAFS was performed using the REX version 2.5 program (RIGAKU). The Fourier transformation of the k^3-weighted EXAFS oscillation from k space to r space was performed over the range 30–140 nm^{-1} to obtain a pseudo-radial distribution function. The inversely Fourier filtered data were analyzed with a non-linear least square curve fitting method in the k range of 30–140 nm^{-1}. For the curve fitting analysis, the phase shift and amplitude functions for the Ag–Cu, Ag–Ag and Ag–O shells were calculated using FEFF program.

Measurements of X-ray photoelectron spectroscopy (XPS) and Auger electron spectroscopy (XAES) were carried out on a JPS-9010MC photoelectron spectrometer equipped with an Al K_α X-ray radiation source ($h\nu$ = 1486.6 eV). Prior to measurements, each sample was pressed into thin disk and pretreated in an atmosphere of 5% H_2-95% Ar (5×10^4 Pa) at 623 K for 1 h in an auxiliary pretreatment chamber. After pretreatment, the sample was introduced into the XPS chamber avoiding exposure to air. The XPS spectra of as-calcined and pretreated samples were recorded at room temperature and the binding energy (BE) were calibrated using C 1s peak at 284.6eV as reference with an uncertainty of ±0.2 eV.

Cu dispersions of the catalysts were determined by dissociative N_2O chemisorption and hydrogen pulse reduction on a Micromeritics Autochem II 2920 apparatus with a TCD. Typically, 100 mg of Cu/SiO_2 calcined at 623 K was reduced in $5\%H_2$-$95\%N_2$ (50 cm^3

min^{-1}) at 623 K for 4 h and cooled to 333 K. Then pure N_2O (30 cm^3 min^{-1}) was introduced for 30 min to completely oxidize surface Cu atoms into Cu_2O. Hydrogen pulse reduction of surface Cu_2O to metallic Cu was conducted at 573 K to ensure that the chemisorbed oxygen can immediately react with high-purity hydrogen supplied from a 0.4 mL loop, and moisture was removed by a 5A zeolite dehydration trap. Hydrogen pulse-dosing was repeated until the pulse area no longer changed. The consumed amount of hydrogen was the value obtained by subtracting the small area of the first few pulses from the area of the other pulses. Cu loading of all reduced catalysts was analyzed by inductively coupled plasma optical emission spectrometry (ICP-OES) on a Thermo Electron IRIS Intrepid II XSP. Cu dispersion was calculated by dividing the amount of chemisorption sites into total supported Cu atom in per gram of catalyst.

2.3. Catalytic testing

Catalytic performance for the DMO hydrogenation was evaluated using a fixed-bed microreactor equipped with a computer-controlled auto-sampling system. As a typical procedure, 200 mg of catalyst precursor (40–60 meshes) was loaded into the center of the reactor with both sides of the catalyst bed packed with quartz powders (40–60 meshes). The catalyst was activated in a flow of 5% H_2-95% N_2 (50 mL min^{-1}) at 623 K for 4 h, with a ramping rate of 2 K min^{-1}. After cooling to reaction temperature, pure H_2 (99.999%) was switched to pass through the catalyst bed, a DMO methanol solution (0.01 g mL^{-1}) was then pumped into the reactor by a Series III digital HPLC pump (Scientific Systems, Inc.) with a

system pressure of 3.0 MPa. The outlet stream was sampled using an automatic Valco 6-ports valve system and analyzed by an online gas chromatograph with a flame ionization detector and a KB-Wax capillary column (30 m × 0.45 mm × 0.85 μm) at intervals of 30 min.

The initial turn over frequency (TOF) of the reaction was measured under the conditions where the DMO conversion was lower than 35%. The TOF value was based on the Cu dispersion or the number of surface metal atoms estimated by metal dispersion according to the equation in previous literature [36], indicating the moles of DMO converted per hour by per mole of metal at the catalyst surface (mol-DMO mol-$metal_{surf}^{-1}$ h^{-1}, for short h^{-1}).

3. Results and discussion

3.1. Catalytic activity and stability

For a rigorous comparison of the catalytic activity between Cu/SiO_2 and Cu_1-Ag_x/SiO_2, the DMO conversion was restrained less than 35% by adjusting the DMO weight liquid hourly space velocity ($WLHSV_{DMO}$) (Table 1). The DMO conversion data were then used to calculate the TOF by DMO conversion according to the Cu dispersion (TOF_{Cu}) and total metal dispersion (TOF_M) as listed in Table 1??~~2~~. The TOF_{Cu} exhibited a volcano-type improvement as the increase of Ag content in Cu_1-Ag_x/SiO_2 and reached a maximum (18.3 h^{-1}) at the Ag/Cu atomic ratio of 0.05/1.The TOF_M of the catalysts presented a tendency similar to TOF_{Cu}, but its value was slightly higher than TOF_{Cu} when the Ag/Cu atomic ratio was below 0.1, indicating that there exist some interactions between Ag and Cu. Further

increasing Ag loading restrained the catalytic activity, and the restriction was more obvious when the monometallic Ag catalyst was taken into account. The results demonstrate that there is a synergistic effect between Cu and Ag for the hydrogenation of DMO to EG.

When the DMO hydrogenation was conducted under the conditions of 1.05 h^{-1} $WLHSV_{DMO}$, 463 K, 3.0 MPa H_2 pressure, and 80 H_2/DMO molar ratio, the bimetallic catalysts employed showed a DMO conversion higher than 97% (Table 1S in the Supporting Information), but Cu/SiO_2 catalyst gave a DMO conversion of 87.2% and30.7% selectivity to EG; $Ag/SiO_2$was almost inactive. That is, Ag incorporated Cu/SiO_2could get a resultant of dramatically improved yield of EG compared with monometallic Cu/SiO_2or Ag/SiO_2.It was noteworthy that the Ag/Cu atomic ratio had a significant effect on tuning the catalytic capability of DMO hydrogenation. Introducing a very small amount of Ag (Ag/Cu atomic ratio = 0.02, Ag loading = 0.26 wt %) into the Cu/SiO_2elevated the EG yield to 58.4%, which was twice as that of monometallic Cu/SiO_2 catalyst. Increasing the Ag/Cu atomic ratio to 0.05, the catalyst thus resulted showed a maximal EG yield of 85.9%. When further increasing the Ag/Cu atomic ratio larger than 0.1, the catalyst gave a lower EG yield.

The catalytic performance of Cu/SiO_2 and optimized Cu_1-$Ag_{0.05}/SiO_2$ catalysts were further investigated under different $WLHSV_{DMO}$ values (Fig. 1). The conversion of DMO remained above 99% over Cu_1-$Ag_{0.05}/SiO_2$ catalyst when $WLHSV_{DMO}$ varied from 0.3 to 1.05 h^{-1}, that over Cu/SiO_2 began to decline when $WLHSV_{DMO}$ was set at 0.6 h^{-1}. The selectivity to EG was kept at about 97% over Cu_1-$Ag_{0.05}/SiO_2$ catalyst, but that over Cu/SiO_2 declined to lower than 50% when $WLHSV_{DMO}$ was up to 0.75 h^{-1}. Accordingly, it is ease to

obtain the EG yield over Cu_1-xAg_x/SiO_2 catalysts as a function of $WLHSV_{DMO}$ (Fig. S1 in the Supporting Information), indicating that the influence of $WLHSV_{DMO}$ was significant and the bimetallic Cu-Ag/SiO_2 catalysts presented much better catalytic performance and tolerance to $WLHSV_{DMO}$ than Cu/SiO_2 for the hydrogenation of DMO.

The long-term catalytic behavior of Cu/SiO_2 and optimized Cu_1-$Ag_{0.05}/SiO_2$ was further evaluated under reaction conditions of 463 K, 3.0 MPa, 80H_2/DMO molar ratio, and 0.6 h^{-1} $WLHSV_{DMO}$. As shown in Fig. 2, the DMO conversion and the EG selectivity of Cu/SiO_2 catalyst dramatically decreased to about 60% and 10% respectively after 100 h, whereas the Cu_1-$Ag_{0.05}/SiO_2$ catalyst retained its initial excellent activity for over 150 h. The results suggested that adding proper amount of Ag into Cu/SiO_2 can not only remarkably enhance the DMO hydrogenation activity, but also effectively improve the catalyst stability.

3.2. Catalyst characterizations

3.2.1.Physicochemical properties of the catalysts

The metal loadings of the catalysts determined by ICP-OES are listed in Table 2. The actual loadings of Cu and Ag were slightly lower than the theoretica lvalue because the metallic ions weakly absorbed on silica gel were eluted during the filtration process. However, the actual atomic ratio of Ag/Cu in the catalysts was close to the preset value. Physicochemical properties of the catalysts are also summarized in Table 2. The introduction of Ag had no obvious effect on the surface area of the catalysts, while the pore volume and average pore diameter slightly increased when the Ag/Cu atomic ratios were lower than 0.1,

then decreased after further introducing silver. Since the reaction of N_2O with metallic Ag species occurs at relatively high temperature (658 K) [37] or needs long reaction time (5 h) if temperature is below 373 K [38], and the Ag content was very low in the present bimetallic catalysts, the concurrent oxidation of metallic Ag species in the process of determination of Cu dispersion by N_2O at 333 K was ignored. Thus, the Cu dispersions of bimetallic Cu-Ag/SiO_2 catalysts are summarized in Table 1. The Cu dispersion increased firstly and was maximized at Ag/Cu atomic ratio of 0.05 with a value of 43.1 m^2 g^{-1}, and then declined mildly with further increasing Ag loading. The results suggested that the introduction of proper amount of Ag facilitated the higher dispersion of Cu particles. It should be noted that the Cu_1-$Ag_{0.05}$/SiO_2 with the highest Cu dispersion presented the optimal catalytic performance under identical reaction conditions.

3.2.2. TEM, EDS and XRD

The morphologies and structural details of the bimetallic catalysts were examined by TEM (Fig. 3). The metal nanoparticles were distributed uniformly on the surfaces of the silica, and the particle diameter distribution showed that mean particle size of all the samples was about 3 nm. High-resolution TEM (HRTEM) of a typical metal particle in the Cu_1-$Ag_{0.05}$/SiO_2 catalyst (Fig. S2 in the Supporting Information) indicated the 0.188 nm [KA1]interval off lattice fringes was smaller than those of the monometallic Ag(111) (0.236 nm), Ag(200) (0.204 nm), and Cu(111) (0.209 nm), but larger than Cu(200) (0.181 nm). The result may be an indication for the formation of Cu-Ag alloy after reduction. The total metal

dispersion of catalysts calculated according to the TEM is listed in Table 2. As can be seen, in line with the trend of Cu dispersion, the total metal dispersion of catalysts improved with increasing Ag/Cu atomic ratio. The dispersion of Cu_1-$Ag_{0.05}/SiO_2$ was maximal with a value of 38.4 $m^2\ g^{-1}$.

The high-angle annular dark-field scanning transmission electron microscopy (HAADF-STEM) images of the as-reduced Cu_1-Ag_x/SiO_2 bimetallic catalysts were shown in Fig. S3 (in the Supporting Information). The tiny bright spots in the images correspond to metal nanoparticles supported on the SiO_2. In combination with X-ray energy dispersive spectroscopy (X-EDS) system equipped with a sub-nanometer probe, we can locate the convergent electron beam (0.5 nm) at any position of the sample to obtain more detail features of metal nanoparticles such as element distribution, composition etc. under HAADF-STEM mode. The compositions of individual metallic particles on the several as-reduced Cu_1-Ag_x/SiO_2 catalysts were measured via point EDS analysis on thirteen metal particles randomly chosen (Fig. S3 in the Supporting Information). The EDS results revealed that both Cu and Ag elements were detectable, and the Ag/Cu atomic ratio was considerably higher than the preset values in most of the metallic particles. The Cu contents were much higher than Ag in Cu_1-Ag_x/SiO_2 catalysts, but the compositions detected by EDS indicated an segregation of Ag species, implying that most of bimetallic particles might be composed of small Ag and Cu-Ag alloy nanoclusters located on the surfaces of Cu NPs. In another word, the results implied that Cu and Ag atoms intimately contacted with each other, providing the premise of the synergistic effects.

The XRD patterns showed that the as-calcined catalysts were amorphous except the Ag/SiO_2 (Fig. S4 in the Supporting Information). Introduction of Ag into Cu/SiO_2 did not significantly change the XRD patterns of Cu/SiO_2 catalyst. Neither Cu nor Ag species could be detected in these precursors, implying that Cu and Ag were highly dispersed on the porous silica support using urea-assisted gelation method. However, well dispersed pure Ag/SiO_2 cannot be prepared by this method.

We then conducted *in situ* XRD characterization to monitor the phase evolution of Cu/SiO_2 and optimized Cu_1-$Ag_{0.05}/SiO_2$ catalysts with increasing reduction temperature under 5%H_2-95%N_2 atmosphere. As shown in Fig. 4, a diffraction peak at 2θ of 43.2°, the characteristic peak of Cu(111) (JCPDS 04-0836), became detectable because some Cu^{2+} species on the Cu/SiO_2 catalyst precursor were reduced to Cu^0 when the reduction temperature raised up to 523 K. According to the Scherrer equation, the Cu crystallite size of Cu/SiO_2 catalyst was smaller than 4 nm when the reduction temperature was lower than 773 K, while the Cu crystallite size of Cu_1-$Ag_{0.05}/SiO_2$ catalyst was smaller than 3.2 nm at the same reduction temperature range. The diffraction peaks of Cu_1-$Ag_{0.05}/SiO_2$ catalyst were to some extent broader than those of the pure Cu catalyst, indicating that adding proper amount of Ag into Cu/SiO_2 catalyst could improve Cu dispersion. This was in accordance with the results of dissociative N_2O chemisorption and TEM. Further increasing the reduction temperature under 5%H_2-95%N_2, the Cu diffraction of both Cu/SiO_2 and Cu_1-$Ag_{0.05}/SiO_2$ peaks became sharper, displaying a similar phase evolution behavior.

After long-term catalytic test, the catalysts were carefully collected under hydrogen atmosphere at room temperature and sealed in glass bottles to protect the samples from oxidation. The XRD diffraction peaks of metallic copper were significant different from each other for the Cu/SiO_2 and Cu_1-$Ag_{0.05}/SiO_2$ catalysts (Fig. S5 in the Supporting Information). The Cu diffraction peak of the spent Cu/SiO_2 catalyst at 2θ of 43.2° was sharper than that of Cu_1-$Ag_{0.05}/SiO_2$. Insignificant changes occurred for the Cu_1-$Ag_{0.05}/SiO_2$ catalyst before and after long-term reaction. Furthermore, TEM images of these catalysts intuitively revealed the consistent results (Fig. S6 in the Supporting Information). Transmigration and aggregation of Cu happened on Cu/SiO_2 after long-term catalytic reaction. Thus, we speculated that Cu agglomeration was one of the key factors to cause the deactivation of the catalyst. Clearly, the addition of Ag played an important role in retarding the aggregation of metallic Cu crystallites.

3.2.3. H_2-TPR

In many case, presence of a noble metal affected the reducibility of surface metal oxides. H_2-TPR characterizations were carried out to investigate the reducibility of the as-calcined samples with different Ag/Cu atomic ratios. There was no obvious reduction peak for the as-calcined Ag/SiO_2 catalyst (Fig. S7 in the Supporting Information). The as-calcined Cu/SiO_2 presented a reduction peak at 518 K, assigned to the reduction of highly dispersed CuO to Cu^0 and copper phyllosilicate to Cu^+ [3,39]. The reduction peaks of bimetallic samples gradually shifted to lower value with the increase of Ag/Cu atomic ratio. The

tendency of Ag introducing to decrease the reduction temperature was consistent with the results reported by Zhou et al. [31], suggesting that some intense interactions between Cu and Ag species occurred.

3.2.4.UV-vis DRS

The UV-vis DRS of as-reduced Ag/SiO_2 catalyst gave a strong absorption peak at 395 nm, which is typical for the well-known surface plasmon resonance (SPR) band of Ag NPs (Fig. S8 in the Supporting Information). Meanwhile, Cu/SiO_2 showed a very weak and broad SPR band around 600 nm. The UV-vis DRS spectra of bimetallic catalysts showed a single SPR bandbetween 400–600 nm, which revealed that it was not a physical mixture of the individual metals [40]. The SPR band gradually shifted to blue range with the increase of Ag/Cu atomic ratio, indicating that the electronic structure of the bimetallic samples changed after silver introducing, because the SPR bands of metal particles are caused by the collective oscillations of the conduction electrons and the d-band energy level continuous changed as a result of an increase in Ag composition [40,41].

3.2.5. XPS and XAES

The XPS was employed to investigate the surface valence state of the as-reduced $Cu\text{-}Ag/SiO_2$ catalysts. For Cu/SiO_2 catalyst, the Cu 2p XPS peaks corresponding to Cu $2p_{3/2}$ and Cu $2p_{1/2}$ appeared at 932.5 eV and 952.4 eV, respectively (Fig. S9 in the Supporting Information). Nevertheless, the BE of Cu $2p_{3/2}$ shifted to higher values with the increase of

Ag content, indicating the electronic effect was more obvious as the Ag content increase. The absence of 2d→3d satellite peaks at 934.9 or 933.5 eV suggested that Cu^{2+} was successfully reduced to Cu^0 and/or Cu^+ after reduction at 623 K [13].

The Ag 3d XPS spectra of the as-reduced Ag/SiO_2 showed typical Ag $3d_{5/2}$ and Ag $3d_{3/2}$ peaks centered at 367.9 eV and 373.9 eV (Fig. S10 in the Supporting Information), which were coincident with the reported values (367.9–368.1 eV and 373.9–374.1 eV) of the metallic Ag [42]. In addition, it was reported that the Ag $3d_{5/2}$ BE of the Ag_2O and AgO were reported at 367.6–367.7eV and 367.2–367.4 eV, respectively [42], which is in contrast to the typical positive core level BE shifts of metal cations in ionic materials. As shown in Fig. S10, the Ag $3d_{5/2}$ peak of the as-reduced bimetallic catalysts shifted to higher BE values compared to the monometallic Ag/SiO_2 catalyst, which implied that Ag species of the bimetallic catalysts had a greater tendency of electronic richness compared with those of monometallic Ag/SiO_2, according to the anomalous spectral shift behavior of silver/silver oxide system.

Since BE value of Cu^0 and Cu^+ species is almost the same, the XAES spectra was conducted to further discriminate the surface Cu^0 and Cu^+ species of the as-reduced Cu_1-Ag_x/SiO_2 catalysts. In the Cu LMM XAES spectra (Fig. 5), asymmetry and overlapped Auger peaks were observed, which strongly indicated that Cu^0 and Cu^+ species were coexisted in the reduced catalysts. The deconvolution results are listed in Table 3. It was obvious that the surface Cu^+ and Cu^0 distributions were significantly affected by the Ag/Cu atomic ratio. The $Cu^+/(Cu^0+Cu^+)$ intensity ratio firstly enhanced and reached the maximized

value of 53.4% at Ag/Cu atomic ratio of 0.05, then dropped mildly with further increasing silver loading.The Auger parameter (AP) of Cu^{+} and Cu^{0} were close to the reported values that 1851.0 eV for Cu^{0} and 1847.0 eV for Cu^{+} [43].

3.2.5. EXAFS

Extended X-ray absorption fine structure (EXAFS) measurements were conducted to further investigate the near-neighbor atomic environment of Cu and Ag. The Fourier transforms of Ag K-edge EXAFS spectra of Cu_1-$Ag_{0.05}/SiO_2$, Ag/SiO_2, and Ag foil are shown in Fig. 6. Obviously, the first nearest neighbor distance of Ag/SiO_2 was close to Ag foil. The Cu_1-$Ag_{0.05}/SiO_2$ catalyst showed a relatively broad peak at a position that is lower than the peak for Ag foil and longer than the peak for Ag_2O at around 2.0 Å [29], implying the existence of a Ag–Cu bond. For Fourier transforms of Cu K-edge EXAFS, the first nearest neighbor distance of Cu/SiO_2 and Cu_1-$Ag_{0.05}/SiO_2$ catalyst showed no obvious difference from that of Cu foil (Fig. 7).

Structural parameters derived from curve fitting analysis are listed in Table 4 and Table S2. For Ag K-edge EXAFS of Cu_1-$Ag_{0.05}/SiO_2$, a Cu–Ag shell at bond distance (R) of 2.64 Å with coordination number (N) of 11 was observed without considering Ag–Ag distance by neglecting the Ag–Ag contribution. When Ag–Ag coordination was taken into account, a Ag–Cu shell at bond distance (R) of 2.63 Å with coordination number (N) of 10 and a Ag–Ag shell at bond distance (R) of 2.89 Å with coordination number (N) of 2.7 were detected. Herein, the Ag–Cu coordination number was corrected by using Ag–Ag ~~coordination~~

~~number~~reduction factor, since we did not have good Ag–Cu reference compound. For Cu_1-$Ag_{0.05}/SiO_2$, the coordination number (N) of Ag–Cu took up 78% of the total coordination number (N) of Ag, which suggested that most of Ag bonded to Cu to form Cu–Ag alloy~~ and a small part of Ag (ca. 22%) formed Ag clusters~~[KA2].~~ The much smaller Ag–Ag coordination number of Cu_1-$Ag_{0.05}/SiO_2$ (2.7) than Ag foil (12) indicating the presence of tiny metallic Ag clusters with sizes below a few nanometers [29]. Moreover, the total coordination number around Ag was nearly 12, indicating that small Ag cluster was mainly surrounded by Cu.~~ For Cu K-edge, Cu_1-$Ag_{0.05}/SiO_2$ sample gave a Cu–Cu shell at bond distance (R) of 2.52 Å with coordination number (N) of 9.2. For the Ag content was just 0.05 and Ag–Cu shell determined from Ag K-edge was just 10, according to the relation of $N_{Ag–Cu} \times C_{Ag} = N_{Cu–Ag} \times C_{Cu}$, the calculated N_{Cu-Ag} was ca. 0.6, which was too small to be detected. The Cu/SiO_2 sample consisted of a Cu–Cu shell (N = 6.2 at R = 2.53 Å) and a weak Cu–O shell (N = 0.8 at R = 1.83 Å), which implied that Cu species was somewhat oxidized.

The Ag K-edge X-ray absorption near-edge structure (XANES) spectra of Cu_1-$Ag_{0.05}/SiO_2$ showed that Ag shifted to lower energy side compared with that of Ag/SiO_2 and Ag foil (not shown), indicating Ag was negatively charged in Cu_1-$Ag_{0.05}/SiO_2$. The result was in good agreement with the aforementioned XPS analysis.

3.2.6 Structure-performance relationship

Based on the analysis of structure characterization results, a possible schematic diagram of Cu_1-Ag_x/SiO_2 catalysts varied with Ag/Cu atomic ratio is proposed and shown in Fig. 8.

Monometalic Cu/SiO_2 catalyst with relatively low Cu dispersion showed poor catalytic activity and stability. After incorporating with a small amount of Ag ($0.02 \leq x \leq 0.05$), a kind of hybrid nanoparticles composed of Cu NPs, Ag nanoclusters, and Ag-Cu alloys are formed on the SiO_2 surfaces. These species are coherently interacted and may play important roles in modulating the Cu^+/Cu^0 ratio and retarding the aggregation of Cu NPs during reaction process. With further increasing the Ag/Cu atomic ratio ($0.1 \leq x \leq 0.2$), excessive Ag nanoclusters cover/block the surface of Cu NPs and disturbed the balance of Cu^+/Cu^0 ratio, resulting in the decrease of the catalytic activity.

Using the catalytic results, the dispersion of Cu and metal, and the Cu^+/Cu^0 ratio, we can discuss the effects of Ag/Cu atomic ratio and Cu^+/Cu^0 on the TOF with respect to the number of surface metal atoms. As shown in Fig. 9, both $Cu^+/(Cu^0+Cu^+)$ intensity ratio and TOF showed a volcano-type dependence on the Ag/Cu atomic ratio, suggesting that suitable proportion of surface Cu^+ and Cu^0 was important to gain remarkable catalytic performance. In other words, adding proper amount of Ag could modulate proportion of surface Cu^+ and Cu^0 to obtain excellent activity and stability for the hydrogenation of DMO.

4. Conclusions

Incorporating a proper amount of Ag into Cu/SiO_2 has been demonstrated significantly enhancing the catalytic activity and stability for the hydrogenation of DMO to EG. The EG yield over the optimized catalyst Cu_1-$Ag_{0.05}/SiO_2$ is 2.2 times higher than that over the monometallic Cu/SiO_2 under the conditions of 463 K, 3.0 MPa, 80 H_2/DMO molar ratio, and

1.05 h^{-1} $WLHSV_{DMO}$. The Cu_1-$Ag_{0.05}/SiO_2$ catalyst can maintain almost 100% DMO conversion and above 97% EG selectivity under the optimized condition for 150 h.

A series of spectroscopic studies including N_2O chemisorption, TEM, *in situ* XRD, EDS, H_2-TPR, UV-vis DRS, XPS, XAES, and EXAFS has been used to explore the structure of the catalysts. Introducing a proper amount of Ag facilitates the higher dispersion of Cu NPs. Parts of Ag species are alloyed with Cu species and others form Ag nanoclusters, both are involved in Cu NPs and coherently interacted with each other on the SiO_2 surface. The distribution of surface Cu^+ and Cu^0 species can be modulated by varying the Ag/Cu atomic ratio. In short, the interactions between Cu and proper amount of Ag species help sustaining the suitable Cu^+/Cu^0 proportion and restraining the transmigration of copper NPs, which are largely responsible for the excellent activity and stability of the bimetallic Cu-Ag/SiO_2 catalyst.

Acknowledgements

We gratefully acknowledge the financial support from the National Basic Research Program of China (2011CBA00508), the Natural Science Foundation of China (20923004 and 21173175), the Research Fund for the Doctoral Program of Higher Education (20110121130002), the Program for Changjiang Scholars and Innovative Research Team in University (IRT1036), and Cooperative Research Program of Catalysis Research Center, Hokkaido University (Grant No. 10B0043).

Appendix A. Supplementary material

Supplementary data associated with this article can be found, in the online version, at doi:10.1016/j.jcat.2013.00.000.

References

[1] H. L.Yue, Y. J. Zhao, X. B. Ma, J. L. Gong, Chem. Soc. Rev. 41 (2012) 4218.

[2] R. A. Kerr, R. F. Service, Science. 309 (2005) 101.

[3] L. F. Chen, P. J.Guo, M. H. Qiao, S. R. Yan, H. X. Li, W. Shen, H. L. Xu, K. N. Fan, J. Catal. 257 (2008)172.

[4] G. H. Xu,Y. C. Li, Z. H. Li, H. J. Wang, Ind. Eng. Chem. Res. 34 (1995) 2371.

[5] Z. N. Xu, J. Sun, C. S. Lin, X. M. Jiang, Q. S. Chen, S. Y. Peng, M. S. Wang, G. C. Guo, ACS Catal. 3 (2013) 118.

[6] D. S. Brands, E. K. Poels, A. Bliek, Appl. Catal. A: Gen. 184 (1999) 279.

[7] L. R. Zehner, R. W. Lenton, US Patent 4 112 245 (1978).

[8] F. Poppelsdorf, Eur. Patent 0 060 787 (1982).

[9] S. Tahara, K. Fujii, K. Nishihira, M. Matsuda, K. Mizutare, US Patent 4 453 026 (1984).

[10] K. Hirai, T. Uda, Y. Nakamura, US Patent 4 614 728 (1986).

[11] H. Miyazaki, K. Hirai, T. Uda, Y. Nakamura, S. Ikezawa, T. Tsuchie, US Patent 57 122 946 (1982).

[12] H. Miyazaki, T. Uda, K. Hirai, Y. Nakamura, H. Ikezawa, T. Tsuchie, US Patent 4 585 890 (1986).

[13] Z. He, H. Q. Lin, P. He, Y. Z. Yuan, J. Catal. 277 (2011) 54.

[14] H. Q. Lin, X. L. Zheng, Z. He, J. W. Zheng, X. P. Duan, Y. Z. Yuan, Appl. Catal. A: Gen. 445–446 (2012) 287.

[15] A. Y. Yin, C. Wen, X. Y. Guo, W. L. Dai, K. N. Fan, J. Catal. 280 (2011) 77.

[16] C. Wen, Y. Y. Cui, A. Y. Yin, K. N. Fan, W. L. Dai, ChemCatChem. 5 (2013) 138.

[17] A. Y. Yin, X. Y. Guo, K. N. Fan, W. L. Dai, ChemCatChem. 2 (2010) 206.

[18] Y. Y. Zhu, S. R. Wang, L. J. Zhu, X. L. Ge, X. B. Li, Z. Y. Luo, Catal. Lett. 135 (2010) 275.

[19] L. Lin, P. B. Pan, Z. F. Zhou, Z. J. Li, J. X. Yang, M. L. Sun, Y. G. Yao, Chin. J. Catal. 32 (2011) 957.

[20] S. R. Wang, X. B. Li, Q. Q. Yin, L. J. Zhu, Z. Y. Luo, Catal. Commun. 12 (2011) 1246.

[21] S. R.Wang, L. J. Zhu, Y. Y. Zhu, X. L. Ge, X. B. Li, Chin. Chem. Lett. 22 (2011) 362.

[22] C. Wen, A. Y. Yin, Y. Y. Cui, X. L. Yang, W. L. Dai, K. N. Fan, Appl. Catal. A: Gen. http://dx.doi.org/10.1016/j.apcata.2013.03.021.

[23] X. Y. Guo, A. Y. Yin, W. L. Dai, K. N. Fan, Catal. Lett. 132 (2009) 22.

[24] A. Y. Yin, X. Y. Guo, W. L. Dai, H. X. Li, K. N. Fan, Appl. Catal. A: Gen. 349 (2008) 91.

[25] A. Y. Yin, X. Y. Guo, W. L. Dai, H. X. Li, K. N. Fan, J. Phys. Chem. C.113 (2009) 11003.

[26] A. Y. Yin, X. Y. Guo, W. L. Dai, K. N. Fan, J. Phys. Chem. C. 114 (2010) 8523.

[27] C. L. Bracey, P. R. Ellis, G. J. Hutchings, Chem. Soc. Rev. 38 (2009) 2231.

[28] X. Y. Liu, A. Q. Wang, L. Li, T. Zhang, C. Y. Mou, J. F. Lee, J. Catal. 278 (2011) 288.

[29] K. Shimizu, K. Shimura, M. Nishimura, A. Satsuma, RSC Adv. 1 (2011) 1310.

[30] J. X. Zhou, L. Y. Guo, X. W. Guo, J. B. Mao, S. G. Zhang, Green Chem. 12 (2010) 1835.

[31] J. W. Zheng, H. Q. Lin, Y. N. Wang, X. L. Zheng, X. P. Duan, Y. Z. Yuan, J. Catal. 297 (2012) 110.

[32] A. Sandoval, A. Aguilar, C. Louis, A. Traverse, R. Zanella, J. Catal. 281 (2011) 40.

[33] A. Y. Yin, C. Wen, W. L. Dai, K. N. Fan, J. Mater. Chem. 21 (2011) 8997.

[34] Y. N. Wang, X. P. Duan, J. W. Zheng, H. Q. Lin, Y. Z. Yuan, H. Ariga, S. Takakusagi, K. Asakura, Catal. Sci. Technol. 2 (2012) 1637.

[35] B. W. Wang, Q. Xu, H. Song, G. H. Xu, J. Nat. Gas Chem. 16 (2007) 78.

[36] J. R. Anderson, Structure of metallic catalysts, Academic Press, New York, 1975.

[37] T. Furusawa, K. Seshan, J. A. Lercher, L. Lefferts, K. Aika, Appl. Catal. B: Enviorn. 37 (2002) 205.

[38] J. J. F. Scholten, J. A. Konvalinka, F. W. Beekman, J. Catal. 28 (1973) 209.

[39] C. J. G. Van Der Grift, A. Mulder, J. W. Geus, Appl. Catal. 60 (1990) 181.

[40] H. T. Beyene, V. S. K. Chakravadhanula, C. Hanisch, T. Strunskus, V. Zaporojtchenko, M. Elbahri, F. Faupel, Plasmonics,7 (2012) 107.

[41] U. Kreibig, M. Vollmer, Optical properties of metal clusters. Springer, Berlin, 1995.

[42] C. D. Wagner, W. M. Riggs, L. E. Davis, J. F. Moulder, in: G. E. Muilenberg (Eds.), Handbook of X-ray Photoelectron Spectroscopy, Perkin–Elmer, Physical Electronics Division, Eden Prairie, Minnesota, 1979.

[43] K. P. Sun, W. W. Lu, F. Y. Qiu, S. W. Liu, X. L. Xu, Appl. Catal. A: Gen. 252 (2003) 243.

Table 1

TOF of Cu_1-Ag_x/SiO_2 catalysts for DMO hydrogenation.[a]

Catalysts	Conversion / %	Selectivity / %		TOF_{Cu}[b] / h^{-1}	TOF_M[c] / h^{-1}
		EG	MG		
Cu/SiO_2	16.0	4.8	95.2	10.1	11.3
Cu_1-$Ag_{0.02}/SiO_2$	22.3	8.2	91.8	13.5	15.1
Cu_1-$Ag_{0.05}/SiO_2$	33.8	8.8	91.2	18.3	20.6
Cu_1-$Ag_{0.1}/SiO_2$	24.5	8.1	91.9	16.1	16.0
Cu_1-$Ag_{0.2}/SiO_2$	16.4	5.1	94.9	13.3	12.1
Ag/SiO_2[d]	3.7	1.6	98.4		5.5

[a] Reaction conditions: T = 463 K, $P(H_2)$ = 3.0 MPa, H_2/DMO molar ratio = 80, $WLHSV_{DMO}$ = 3.6 h^{-1}.

[b] TOF_{Cu} was calculated by Cu dispersion.

[c] TOF_M was calculated by metal dispersion.

[d] $WLHSV_{DMO}$ = 1.05 h^{-1}.

Table 2

Physicochemical properties of Cu_1-Ag_x/SiO_2 catalysts.

Catalysts	Cu loading[a] / wt%	Ag loading[a] / wt%	Ag/Cu molar ratio	S_{BET} / $m^2\ g^{-1}$	V_{pore} / $cm^3\ g^{-1}$	D_{pore}/ nm	Cu dispersion[b] / %	Metal dispersion[c] / %
Cu/SiO_2	8.7	-	-	224.5	0.82	12.5	35.3	31.6
Cu_1-$Ag_{0.02}/SiO_2$	8.3	0.26	0.018	216.9	0.90	13.8	38.6	33.8
Cu_1-$Ag_{0.05}/SiO_2$	7.9	0.65	0.048	225.0	0.90	13.7	43.1	38.4
Cu_1-$Ag_{0.1}/SiO_2$	7.3	1.2	0.097	216.6	0.96	14.9	40.5	37.2
Cu_1-$Ag_{0.2}/SiO_2$	6.6	2.0	0.18	187.7	0.63	12.1	36.3	33.8
Ag/SiO_2	-	9.1	-	109.4	0.45	15.2	-	7.1
SiO_2	-	-	-	108.2	0.34	9.9	-	-

[a] Determined by ICP-OES analysis.

[b] Determined by N_2O surface oxidation.

[c] Determined by TEM.

Table 3

Cu LMM deconvolution results of Cu/SiO_2 and Cu_1-Ag_x/SiO_2 catalysts.

Catalyst	K.E.[a]/ eV		A.P.[b]/ eV		Cu $2p_{3/2}$	X_{Cu^+}[c] / %
	Cu^+	Cu^0	Cu^+	Cu^0	B.E. / eV	
Cu/SiO_2	914.0	918.1	1846.5	1850.6	932.5	38.3
Cu_1-$Ag_{0.02}/SiO_2$	914.2	918.1	1486.9	1850.8	932.7	40.7
Cu_1-$Ag_{0.05}/SiO_2$	914.0	917.9	1486.8	1850.7	932.8	53.4
Cu_1-$Ag_{0.1}/SiO_2$	913.9	918.0	1846.8	1850.9	932.9	46.4
Cu_1-$Ag_{0.2}/SiO_2$	913.9	917.9	1846.8	1850.8	932.9	40.9

[a] Kinetic energy.

[b] Auger parameter.

[c] Intensity ratio between Cu^+ and (Cu^+ + Cu^0) by deconvolution of Cu LMM XAES spectra.

Table 4

Curve fitting analysis of Ag K-edge EXAFS of Cu_1-$Ag_{0.05}/SiO_2$, Ag/ SiO_2 and Ag foil.

Sample	Shell	N[a]	R[b] / Å	E[c]/ eV	σ[d] / Å	R_f[d]
Cu_1-$Ag_{0.05}/SiO_2$	Ag–Cu	11	2.64	2.2	0.082	0.029
Cu_1-$Ag_{0.05}/SiO_2$	Ag–Cu	10	2.63	1.5	0076	0.012
	Ag–Ag	2.7	2.89	4.1	0.083	
Ag/ SiO_2	Ag–Ag	8.9	2.85	3.6	0.081	0.052
Ag foil	Ag–Ag	12	2.85	2.8	0.082	0.044

[a] Coordination number.

[b] Bond distance between absorber and backscatter atoms.

[c] Inner potential correction to account for the difference in the inner potential between the sample and the reference compound.

[d] Debye–Waller factor.

[e] Residual factor.

Figure Captions

Fig. 1 DMO hydrogenation over Cu/SiO_2 and Cu_1-$Ag_{0.05}/SiO_2$ catalysts as a function of $WLHSV_{DMO}$. Reaction conditions: T= 463 K, *P* (H_2) = 3.0 MPa, H_2/DMO molar ratio = 80.

Fig. 2 DMO hydrogenation over Cu/SiO_2 and Cu_1-$Ag_{0.05}/SiO_2$ catalysts as a function of time on stream. Reaction conditions: T=463 K, *P*(H_2) = 3.0 MPa, H_2/DMO molar ratio = 80, $WLHSV_{DMO} = 0.6\ h^{-1}$.

Fig. 3 TEM images of as-reduced catalysts. (a) Cu/SiO_2, (b) Cu_1-$Ag_{0.02}/SiO_2$, (c) Cu_1-$Ag_{0.05}/SiO_2$, (d) Cu_1-$Ag_{0.1}/SiO_2$, and (e) Cu_1-$Ag_{0.2}/SiO_2$.

Fig. 4 *In situ* XRD patterns of as-calcined catalysts as a function of reduction temperature under 5% H_2-95% N_2 atmosphere. (a) Cu/SiO_2 and (b) Cu_1-$Ag_{0.05}/SiO_2$.

Fig. 5 Cu LMM XAES spectra of the as-reduced Cu_1-Ag_x/SiO_2 catalysts with different Ag/Cu atomic ratios. (a) Cu/SiO_2, (b) Cu_1-$Ag_{0.02}/SiO_2$, (c) Cu_1-$Ag_{0.05}/SiO_2$, (d) Cu_1-$Ag_{0.1}/SiO_2$, and (e) Cu_1-$Ag_{0.2}/SiO_2$.

Fig. 6 (A) Fourier transforms and (B) k^3-weighted (k) of Ag K-edge EXAFS for (a) Ag foil, (b) Ag/SiO_2, and (c) Cu_1-$Ag_{0.05}/SiO_2$.

Fig. 7 (A) Fourier transforms and (B) k^3-weighted (k) of Cu K-edge EXAFS for (a) Cu foil, (b) Cu/SiO_2, and (c) Cu_1-$Ag_{0.05}/SiO_2$.

Fig. 8 Schematic diagram of Cu_1-Ag_x/SiO_2 catalysts varied with Ag/Cu atomic ratio.

Fig. 9 TOF and $Cu^+/(Cu^0+Cu^+)$ intensity ratio as a function of Ag/Cu atomic ratio.

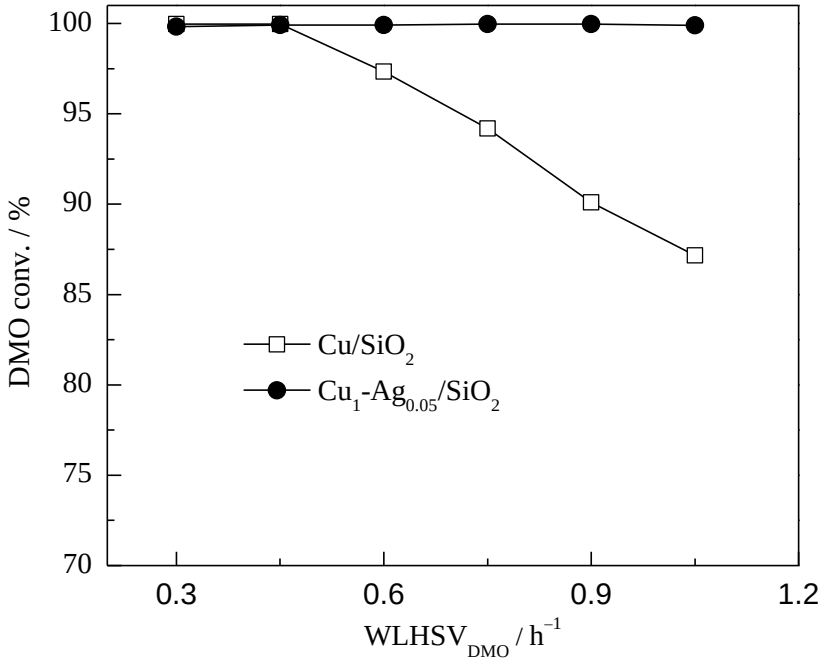

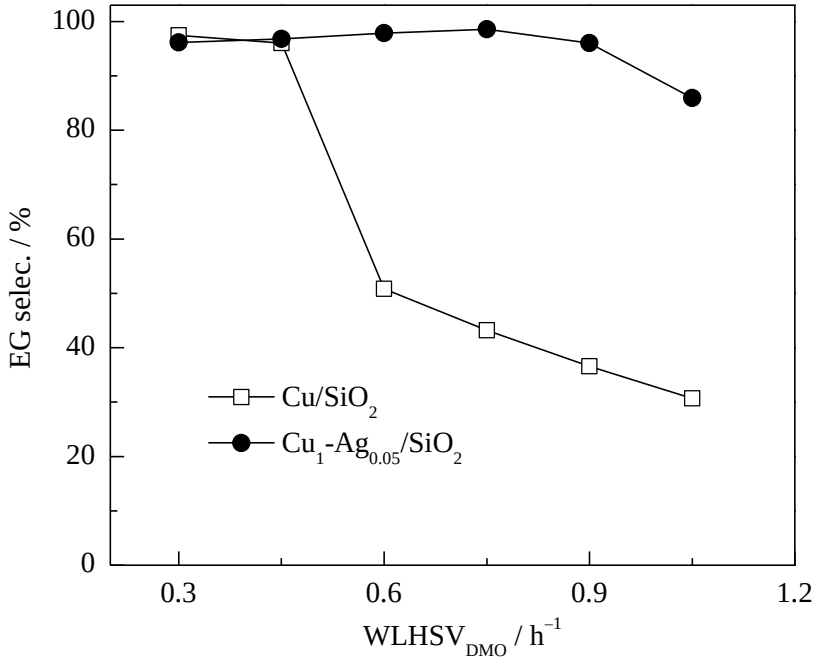

Fig. 1 DMO hydrogenation over Cu/SiO_2 and Cu_1-$Ag_{0.05}/SiO_2$ catalysts as a function of $WLHSV_{DMO}$. Reaction conditions: T= 463 K, *P* (H_2) = 3.0 MPa, H_2/DMO molar ratio = 80.

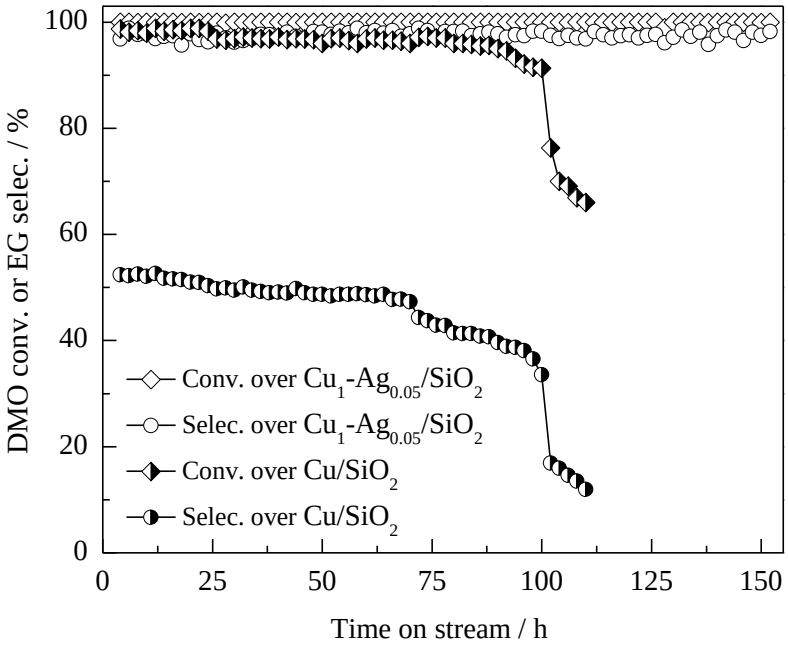

Fig. 2 DMO hydrogenation over Cu/SiO_2 and Cu_1-$Ag_{0.05}/SiO_2$ catalysts as a function of time on stream. Reaction conditions: T=463 K, $P(H_2)$ = 3.0 MPa, H_2/DMO molar ratio = 80, $WLHSV_{DMO}$ = 0.6 h^{-1}.

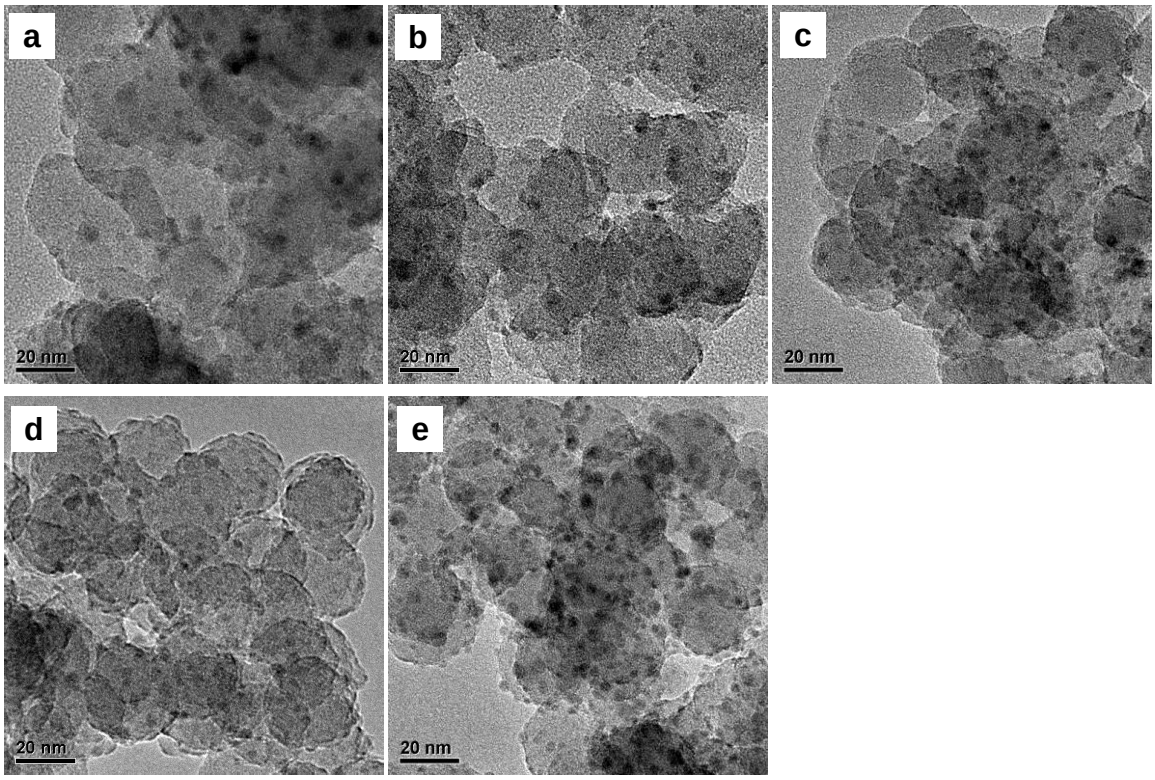

Fig. 3 TEM images of as-reduced catalysts. (a) Cu/SiO_2, (b) Cu_1-$Ag_{0.02}/SiO_2$, (c) Cu_1-$Ag_{0.05}/SiO_2$, (d) Cu_1-$Ag_{0.1}/SiO_2$, and (e) Cu_1-$Ag_{0.2}/SiO_2$.

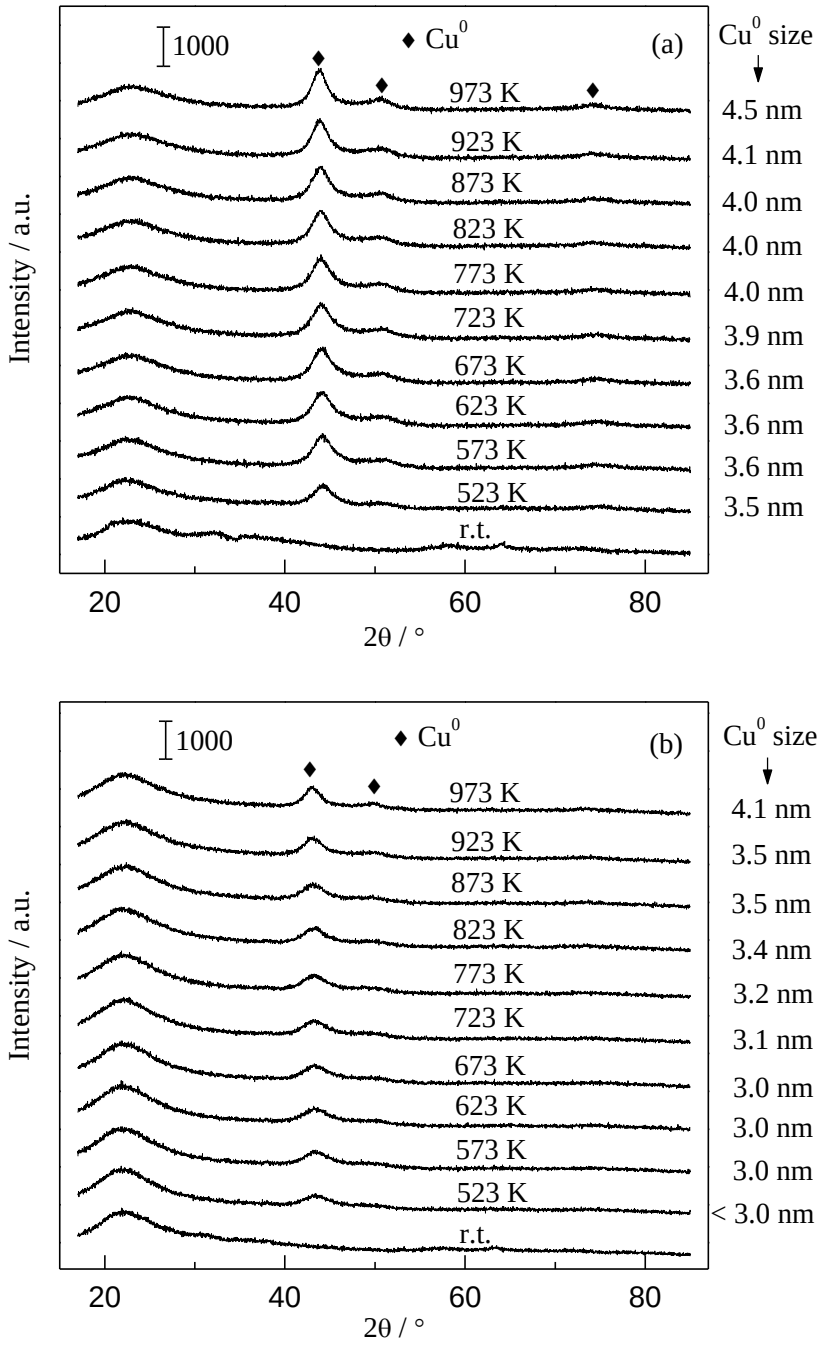

Fig. 4 *In situ* XRD patterns of as-calcined catalysts as a function of reduction temperature under 5% H_2-95% N_2 atmosphere. (a) Cu/SiO_2 and (b) Cu_1-$Ag_{0.05}/SiO_2$.

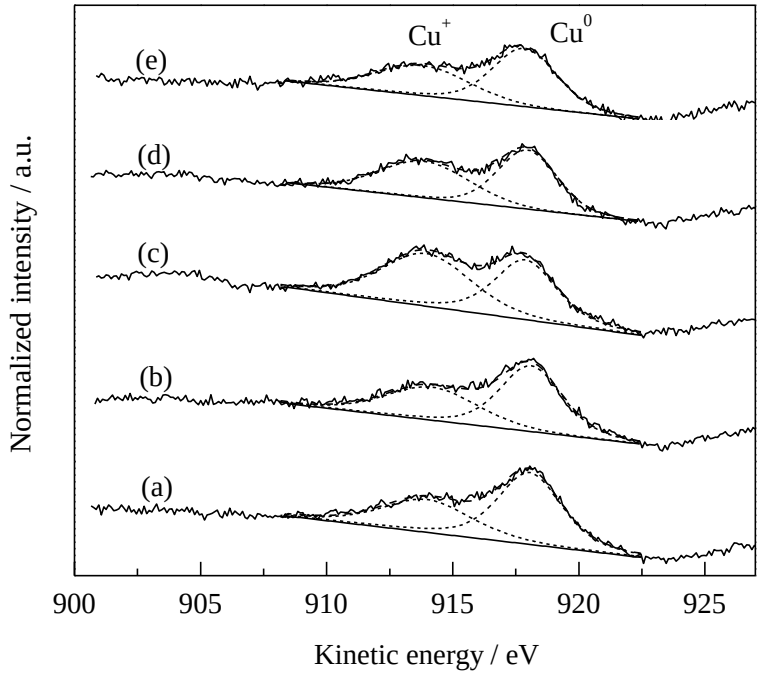

Fig. 5 Cu LMM XAES spectra of the as-reduced Cu_1-Ag_x/SiO_2 catalysts with different Ag/Cu atomic ratios. (a) Cu/SiO_2, (b) Cu_1-$Ag_{0.02}/SiO_2$, (c) Cu_1-$Ag_{0.05}/SiO_2$, (d) Cu_1-$Ag_{0.1}/SiO_2$, and (e) Cu_1-$Ag_{0.2}/SiO_2$.

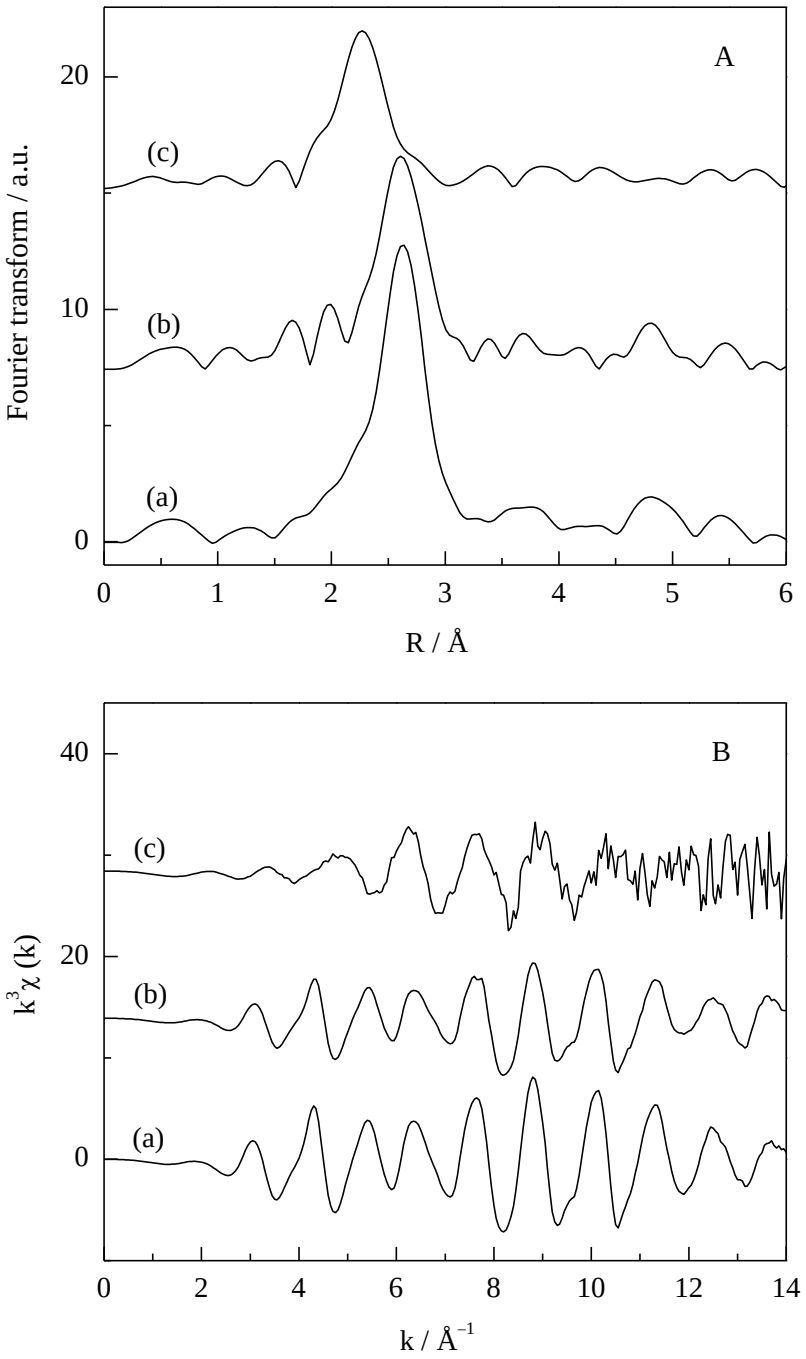

Fig. 6 (A) Fourier transforms and (B) k^3-weighted (k) of Ag K-edge EXAFS for (a) Ag foil, (b) Ag/SiO_2, and (c) Cu_1-$Ag_{0.05}/SiO_2$.

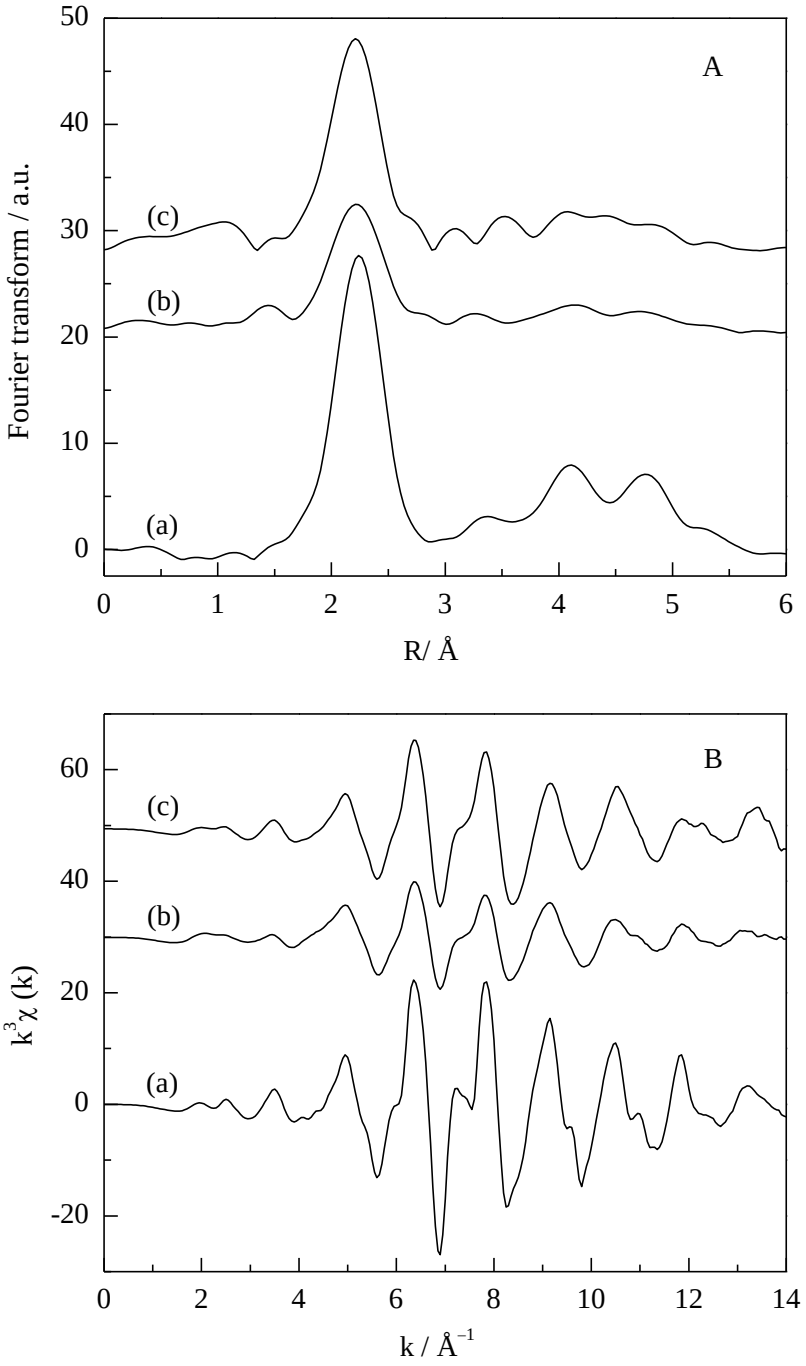

Fig. 7 (A) Fourier transforms and (B) k^3-weighted (k) of Cu K-edge EXAFS for (a) Cu foil, (b) Cu/SiO_2, and (c) Cu_1-$Ag_{0.05}/SiO_2$.

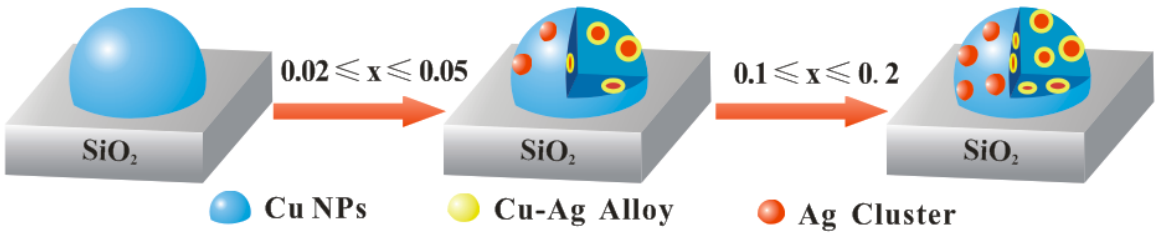

Fig. 8 Schematic diagram of Cu_1-Ag_x/SiO_2 catalysts varied with Ag/Cu atomic ratio.

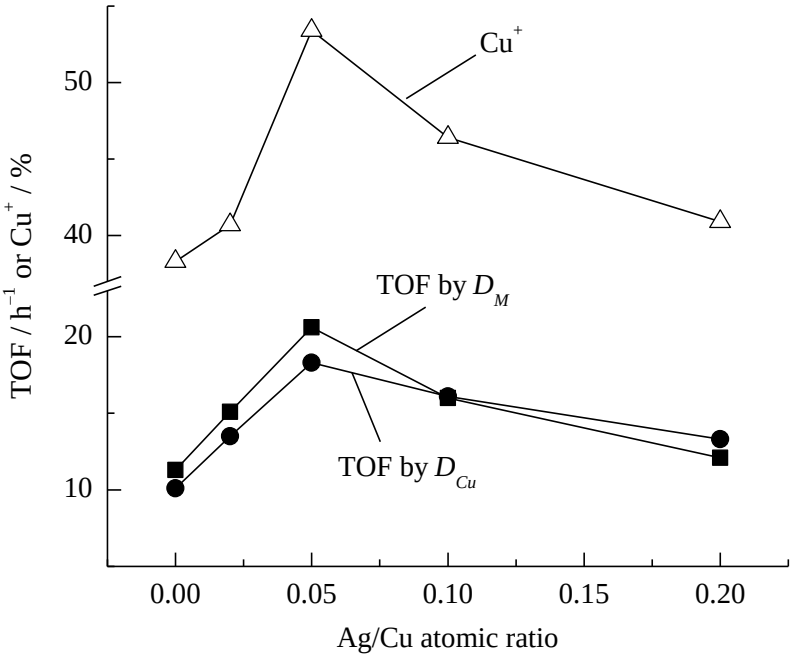

Fig. 9 TOF and $Cu^+/(Cu^0+Cu^+)$ intensity ratio as a function of Ag/Cu atomic ratio.